METEOR-Berichte

Geological and geophysical characterization of transform offsets, TRANSFORMERS

Cruise No. M170

11.01.2021 – 14.02.2021

Emden (Germany) – Emden (Germany)

TRANSFORMERS

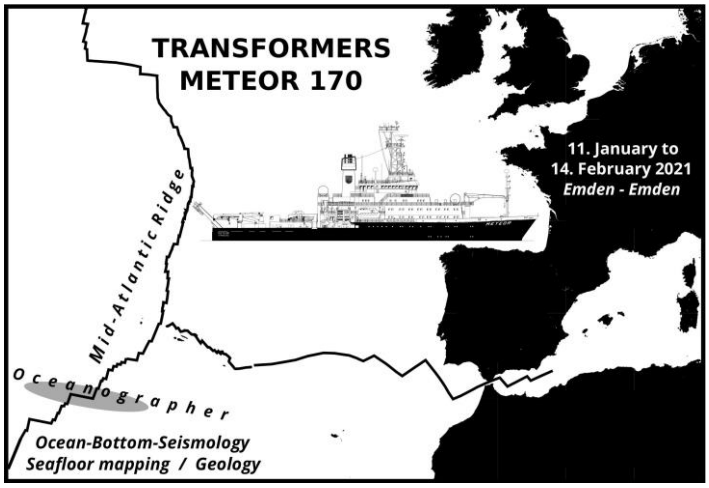

Ingo Grevemeyer, Colin W. Devey, Ingo Klaucke and Dietrich Lange

Ingo Grevemeyer

GEOMAR Helmholtz Centre for Ocean Research Kiel

2021

Table of Contents

1 Cruise Summary

1.1 Summary in English

Fracture zones were recognized to be an integral part of the seabed long before plate tectonics was established. Later, plate tectonics linked fracture zones to oceanic transform faults (OTF), suggesting that they are the inactive and hence fossil trace of transforms. Yet, scientists spend little time surveying them in much detail. Recent evidence suggests that the traditional concept of transform faults as being conservative (non-accretionary) plate boundary faults might be wrong. Instead, numerical modelling results suggest that transform faults seem to suffer from extensional tectonics below their strike-slip surface fault zone, and a global compilation of legacy bathymetric data suggest that ridge-transform intersections seem to be settings of magmatic activity, modifying the lithosphere and burying the transform valley before it passes into the fracture zone region. During M170 we tested those hypotheses by collecting a suite of new data from the Oceanographer and Hayes transform faults offsetting the Mid-Atlantic Ridge to the south of the Azores near 35°N and hence conducted a pilot study revealing the state-of-stress derived from micro-earthquakes and bathymetry as well as geological sampling to evaluate magmatic and tectonic processes shaping transform faults. Preliminary analysis of 10-days of seismicity data recorded at hydrophone stations showed 10-15 local earthquakes per day and bathymetric data supports that ridge-transform intersections support indeed a second phase of magmatic accretion.

1.2 Zusammenfassung

Ozeanischen Bruchzonen wurden in bathymetrischen Daten entdeckt lange bevor die Theorie der Plattentektonik entwickelt wurde. Nach Einführung der Plattentektonik wurden Bruchzonen als der inaktive Teil ozeanischer Transformverwerfungen (OTF) definiert. In den letzten Jahrzehnten fanden Bruchzonen jedoch wenig Beachtung. Von uns durchgeführte Untersuchungen deuten jedoch darauf hin, dass Transformverwerfungen nicht – wie in der Plattentektonik beschreiben – konservative Plattengrenzen darstellen. Numerische Modellierungen deuten darauf hin, dass Transformverwerfungen unterhalb der Blattverschiebungszone eine Region ausbilden in welcher Extension dominiert. Darüber hinaus deuten bathymetrische Daten darauf hin, dass an ihren Enden magmatische Prozesse in einer zweiten Akkretionsphase neue Kruste generieren und somit die Transform Zone magmatisch überprägen. Die Expedition M170 überprüfte diese Hypothesen durch die Aufnahme neuer Datensätze an der Oceanographer Transformverwerfung am Mittelatlantischen Rücken bei 35°N südlich der Azoren. Hierzu wurden sowohl in einer ersten Pilotstudie lokale Erdbeben registriert, um das Spannungsfeld abzuleiten, als auch bathymetrische Daten und geologische Beprobungen vorgenommen, um magmatische Prozesse zu evaluieren. Erste Ergebnisse zeigen, dass über einen Zeitraum von 10 Tagen zwischen 10-15 lokale Mikro-Erdbeben pro Tag im Bereich der Transformverwerfung stattfanden. Darüber hinaus stützen die Kartierungen die These, dass die Nahtstellen zwischen Transformverwerfung und Mittelatlantischen Rücken in der Tat durch magmatische Aktivität charakterisiert sind.

2 Participants

2.1 Principal Investigators

Name	Institution
Grevemeyer, Ingo, Prof.	GEOMAR
Devey, Colin W., Prof.	GEOMAR
Klauke, Ingo, Dr.	GEOMAR
Lange, Dietrich, Dr.	GEOMAR

2.2 Scientific Party

Name	Discipline	Institution
Grevemeyer, Ingo, Prof.	Marine seismology / Chief Scientist	GEOMAR
Devey, Colin, Prof.	Marine geology /Co-Chief Scientist	GEOMAR
Klaucke, Ingo, Dr.	Seafloor imaging & bathymetry	GEOMAR
Lange, Dietrich, Dr.	Marine seismology, OBS	GEAOMR
Bartles, Thies	OBS technician/engineer	GEOMAR
Gómez de la Peña, Laura, Dr.	OBS	GEOMAR
Beniest, Anouk, Dr.	OBS & geology	GEOMAR
Filbrandt, Christian	OBS, student	GEOMAR/CAU
Hilbert, Helene-Sophie	OBS & bathymetry	GEOMAR
Unger, Katharina	Marine geology & bathymetry	GEOMAR
Murray-Berquist, Louisa	OBS & bathymetry	GEOMAR
Ren, Yu	OBS & bathymetry	GEOMAR
Li, Yuhan	OBS & bathymetry	GEOMAR
Hagen, Anna	Geology & bathymetry, student	GEOMAR/CAU
Stiller, Maike	OBS, geology, bathymetry, student	GEAOMR/CAU
Raeke, Andreas	Meteorology technician	DWD

2.3 Participating Institutions

GEOMAR	Helmholtz-Zentrum für Ozeanforschung Kiel
CAU	Christian-Albrechts-Universität zu Kiel
DWD	Deutscher Wetterdienst, Geschäftsfeld Seeschifffahrt

3 Research Program

3.1 Description of the Work Area

3.1.1 Scientific Background - Transform faults revisited

Oceanic fracture zones (FZ) are perhaps the most striking features in the ocean basins, especially in the Pacific Ocean where they were discovered by H. William Menard (1955) long

before the theory of plate tectonics emerged. Seafloor mapping indicated that they are several thousand of kilometres long and have irregular topography, including "great seamounts, narrow troughs, asymmetric ridges and escarpments" (Menard, 1955) for which Menard coined the term "fracture zones". He further noted that they follow small circles, and hence are linear features. They cover roughly 5% of the seafloor in the North Pacific. The longest fracture zone is the Clipperton fracture zone which can be followed for over 10.000 km and hence a quarter of Earth's circumference (Menard, 1967). Today, we know that fracture zones can be easily followed in space geodetic altimetry, confirming that they are indeed the longest linear features on Earth's surface (Sandwell et al., 2014).

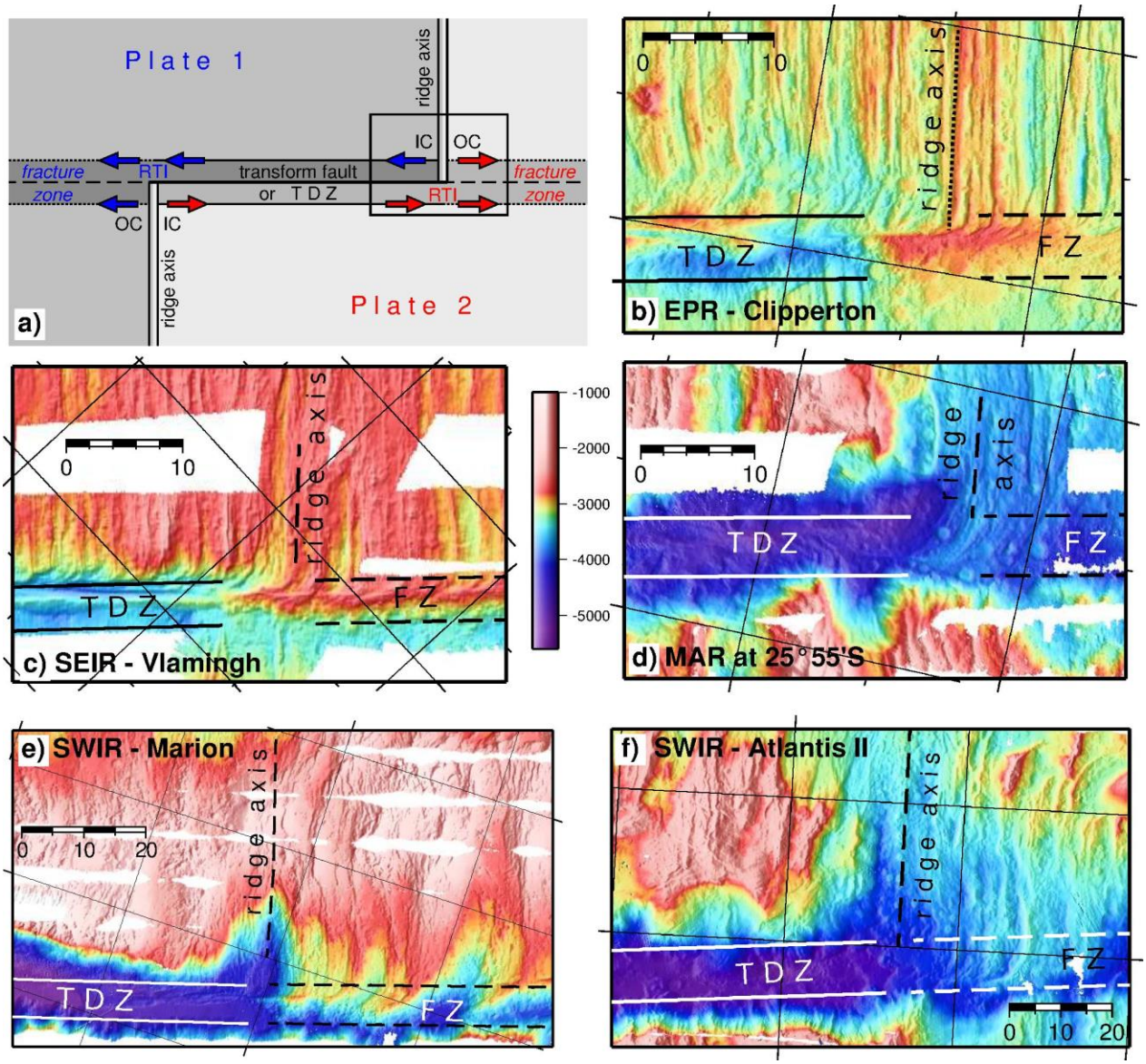

Fig. 3.1. Selected Ridge-Transform-Intersections (RTIs) at a range of spreading rates. a) Cartoon showing the geometry of a transform-fracture zone system; OC: outside corner, IC: inside corner. Bathymetry from RTIs marked by rectangle in a) is shown in b) to f).b) Eastern Clipperton RTI at the fast-spreading Northern East Pacific Rise; b) Southern RTI of the Vlamingh transform at the intermediate-spreading Southeast Indian Ridge; d) Eastern RTI of a transform fault at the slow-spreading Southern Mid-Atlantic Ridge near 25°40'S; e) northern RTI of the Marion transform at the ultraslow-spreading Southwest Indian Ridge; f) southern RTI of the Atlantis II transform at the ultraslow-spreading Southwest Indian Ridge (from Grevemeyer et al., 2021).

Plate tectonics placed fracture zones into a new framework (Fig. 3.1a), showing that they are generically related to oceanic transform faults (Wilson, 1965). Thus, their tectonically active regions (Fig. 1a) is known today as an oceanic transform fault (OTF), where two tectonic plates move past each other (Wilson, 1965). Transform faults are one of the major plate boundary types on the planet, with a total length of 48,000 km (Bird, 2003). Each oceanic transform is bounded by two ridge-transform intersections (RTI) where tectonic stresses rotate by tens of degrees over a very short distance (Morgan and Parmentier, 1994). RTIs separate normal faulting at the mid-ocean ridge (MOR) spreading axis from strike-slip faulting along the transform fault (Sykes, 1967). In the original framework of plate tectonics, transform faults and fracture zones are proposed to be conservative, two-dimensional features that juxtapose lithosphere of contrasting age (Wilson, 1965), leading to flexural adjustment and differential subsidence with age across a fracture zone (e.g., Sandwell, 1984).

Once formed at an RTI, magmatic crust was proposed to traverse the transform with no further modification, becoming part of the fracture zone after passing the opposite RTI (Fox and Gallo, 1984). This model, however, is overly simplified. The active transform domain is not a simple linear fault, but a region several kilometres wide (Fox and Gallo, 1984; Searle et al., 1996; Karson and Dick, 1983), with the active zone ("tectonic deformation zone" - TDZ) showing surface strike-slip faulting along a single fault or a narrow zone of interconnected faults within the transform valley (e.g., Fox and Gallo, 1984; Searle et al., 1996). A re-assessment of bathymetric data and a model-based approach, which we summarize below, supports the idea that transform faults are not conservative plate boundaries. Instead, lithosphere traversing a transform fault is subject to both cross-transform extension that causes the transform valley to be deeper than adjacent seafloor and magmatic addition of new crust as it passes the opposing RTI resulting in seafloor shallowing (Grevemeyer et al., 2021).

Observational constraints

In a global study, surveying the structure of oceanic transform faults and fracture zones, archived high-resolution digital bathymetric data from 41 transform faults and fracture zones (see Fig. 3.1 for examples) show processes at transform faults acting independently of spreading rate. The results of this work (Grevemeyer et al., 2021), which imply that oceanic transform faults do not act as conservative plate boundaries, are briefly presented here.

Most striking is the observation that, independent of spreading rate, the seafloor within the active transform valley is always deeper than that of its immediately adjacent fracture zones. At the fast-slipping Clipperton transform fault at 10°N on the East Pacific Rise (Fig. 3.1b), the depth change occurs at the RTI, where the seafloor is characterized by curving ("J-shaped") volcanic ridges and volcanic structures, called "rooster combs", on the older plate (Gallo et al., 1986, Barth et al., 1994). Very similar bathymetric features (depth change at RTI, J-shaped ridges and/or volcanic cones on the older plate) are found at other transforms faults around the globe, covering the whole range of spreading rates, including slow and ultra-slow slipping transforms (Figs. 3.1d – 3.1f; Grevemeyer et al., 2021).

Statistical characterization of the bathymetry of all 41 studied transform fault systems (Fig. 3.2) reveals that the transform-fracture zone depth difference is an intrinsic feature of transform-fracture zone systems (Fig. 3.2a) and exactly the opposite of predictions of thermal subsidence due to plate cooling (Davis and, 1974) as the older seafloor becomes shallower. Interestingly, the

magnitude of this depth difference does not scale in a simple way with spreading-rate although slower slipping systems tend to show larger depth changes (Fig. 3.2b). Instead, transform valley depth appears to be a function of spreading rate (Fig. 3.2c) and in particular of age-offset at the RTI (Fig. 3.2d).

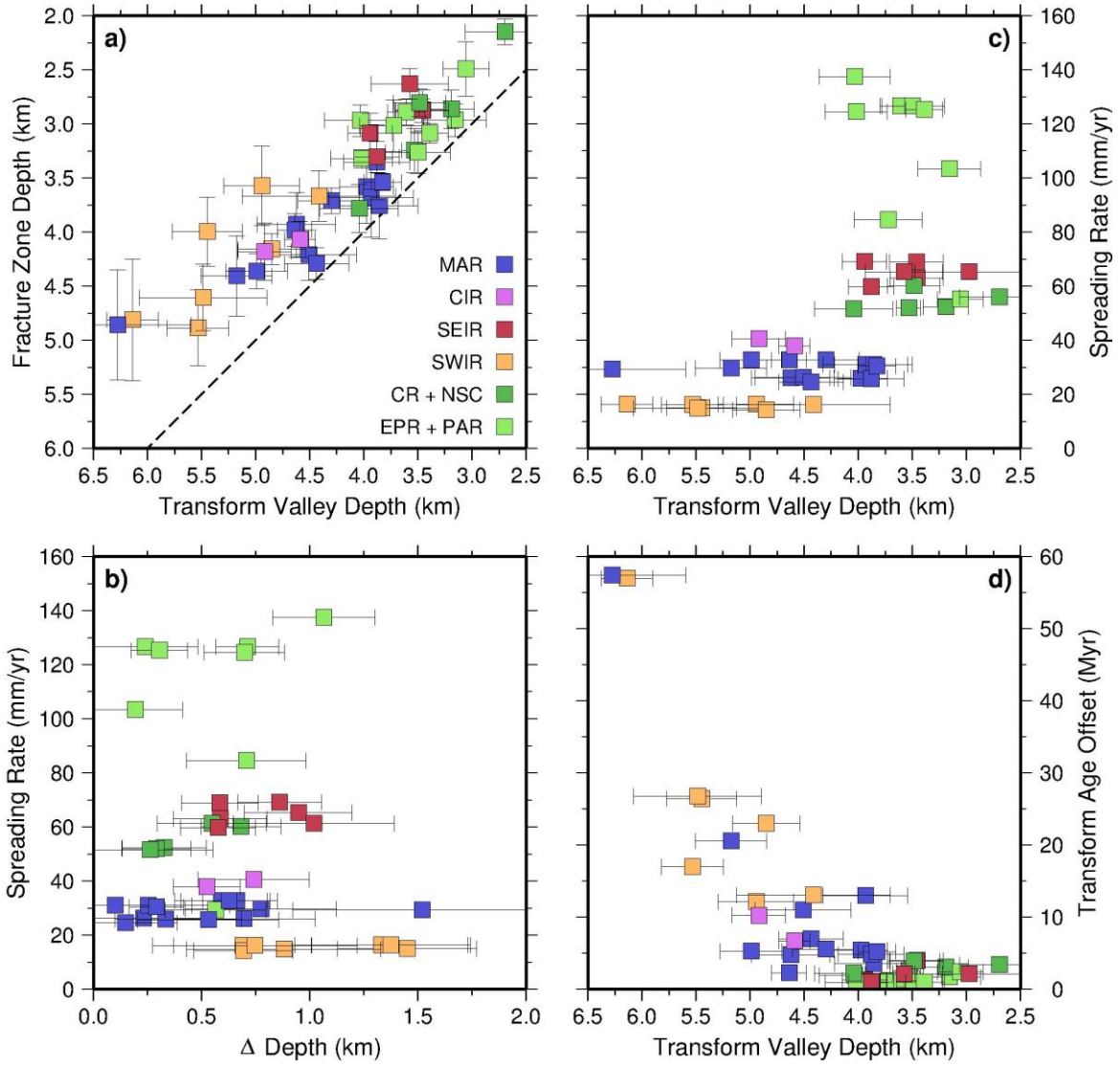

Fig. 3.2. Transform fault and Fracture Zone depth statistics. a) Depth of transform valley versus depth of the valley of the inactive fracture zone just outside the RTI; b) Difference between the transform valley and fracture zone depths in (a) as a function of spreading rate (broken line is one-to-one relationship); c) Transform valley depth as a function of spreading rate; d) Transform valley depth as a function of age-offset. MAR: Mid-Atlantic Ridge, CIR: Central Indian Ridge, SEIR: Southeast Indian Ridge, SWIR: Southwest Indian Ridge, PAR: Pacific Antarctic Ridge, CR: Chile Ridge, EPR: East Pacific Ride. Error bars are root mean square (rms) values of measurements (from Grevemeyer et al., 2021).

Across-transform extension

To further investigate the processes behind transform fault structure, Grevemeyer et al. (2021) used 3-dimensional geodynamic models of flow in mantle with a non-linear visco-plastic

rheology beneath a ridge-transform- ridge system (Fig. 3.3). Results show that the mantle flow at depth, driven by a lithospheric kinematic strike-slip boundary condition at an orthogonal surface transform fault, does not exactly mimic the rectilinear plate boundary. Instead, it organizes itself into a slightly oblique extensional shear zone with an obliquity of 4-16° with respect to the surface expression of the transform (Fig. 3.4a). The difference in age (and hence strength) of plates moving in opposite directions beneath the IC causes drag-induced yielding within the

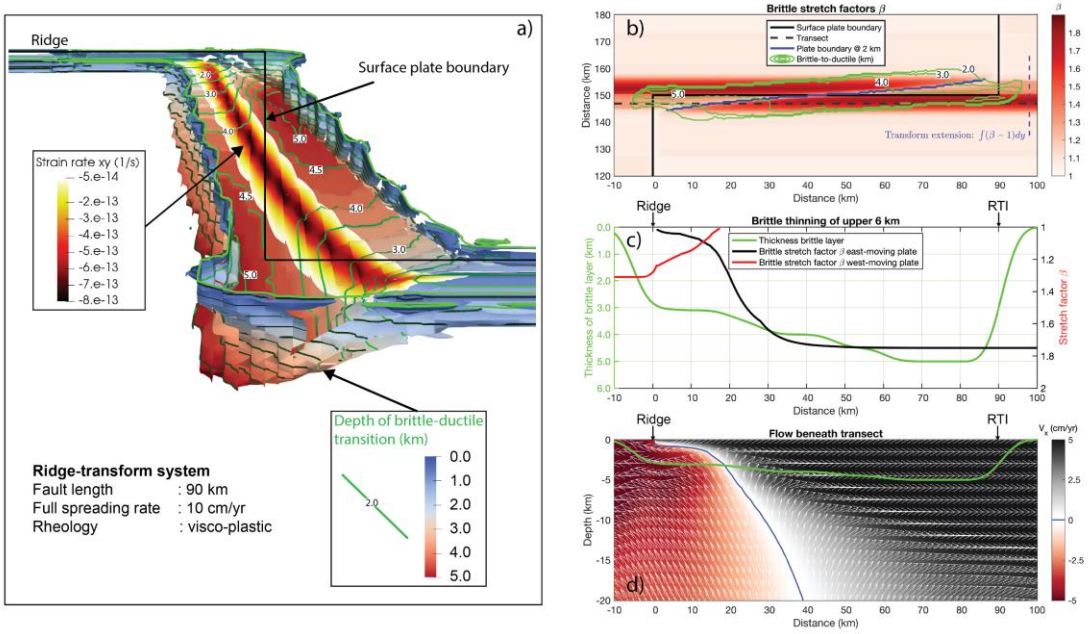

Fig. 3.3. Results of a 3-D viscoplastic geodynamic flow model (model setup is shown in Extended Data Figure 3) using parameters for the Clipperton Transform Fault system. (a) A perspective view of the model transform system of orientation, showing the surface plate boundary (black line), the base of the brittle deformation zone (defined as the zone where stresses are on the brittle yield stress as given by the Drucker-Prager plasticity model used) both as depth contours (green) and a coloured surface (blue-orange scale), and the shear (xy) strain rate at the brittle-ductile transition (shown by a black-yellow "flame" colour scale). (b) Plan view of the model shown in (a) with colour coding for the stretching factor β. (c) Vertical profile through (b) along the dashed black line parallel to the transform showing the depth of the base of the brittle zone (green line, green scale), and the cumulative stretch factor (β) for the west- (red) and east- (black) moving plate. (d) Material flow direction (arrows) and in-profile horizontal velocity (colours) for the same section as in (c) (section location shown in (b)). (from Grevemeyer et al., 2021).

younger plate and flow at depth to be directed in the opposite direction to surface plate motion (Figs 3.3 and 3.4a). This creates sub-horizontal shear and extension within the young transform lithosphere both along the slightly oblique sub-surface transform and at the IC, creating a deep transform valley as a consequence of lithospheric stretching.

The degree of predicted depth-dependent obliquity between the surface transform and the axis of zero horizontal mantle flow at depth is a function of slip rate and transform length, with the along-axis width of the transform 'stretching zone' being a function of age offset only. The magnitude of predicted across-transform extension is also a function of age-offset and is of order of 10s of kilometres (Fig. 3.4b), occurring at rates of 4-20 mm/yr.

Evidence for across-transform extension at some transform faults is also provided in the form of micro-seismicity. At the Kane Transform, ocean-bottom-seismometers (Wilcock et al., 1990) recordings revealed a number of small magnitude normal faulting earthquakes and hence evidence for stretching, which is corroborated by the presence of both strike-slip and tensile earthquakes with magnitudes exceeding 5.5 at major transform systems in the equatorial Atlantic (Wolfe et al., 1993). Further, with decreasing spreading rate increases the thickness of the brittle lithosphere along transform faults. Thus, at fast and intermediate spreading ridges, earthquakes occur at 5-10 km depth (McGuire et al. 2012, Braunmiller and Nablek, 2008), while at the slow slipping large offset equatorial Atlantic transforms they occur at 9-20 km depth (Abercrombie and Ekström, 2001, Grevemeyer, 2020; Wolfe et al., 1993).

RTI magmatism

In contrast, bathymetric data show not only that a pronounced transform valley-fracture zone depth change occurs near the RTI, but that this shallowing is clearly linked to a second phase of episodic magmatic activity as transform seafloor passes the opposing ridge axis (Grevemeyer et al., 2021). In many cases, J-shaped ridges, hummocks, and small volcanic cones extend across the RTI, fully or partially covering the outside corner-fracture zone region, and often terminating in the older plate. These J-shaped ridges appear to be formed by the progressively oblique prolongation of the spreading centre across the transform fault region (Figs 3.4c and 3.4d). This phenomenon has been previously noted at fast and intermediate spreading ridges (e.g., Lonsdale, 1986), but our bathymetric compilation shows that it actually occurs at all spreading rates (see Figs. 3.1c-f and 3.4c & d). At the East Pacific Rise, J-shaped ridges are generally associated with intersection highs across the RTI where the older lithosphere and the opposing ridge tip are juxtaposed (Fox and Gallo, 1984; Gallo et al., 1986; Barth et al., 1994) (Fig. 3.1b, 3.1c,). The RTI volcanic highs are often topped by a carapace of young lavas (Gallo et al., 1986: Barth et al., 1994) and seismic data from the Clipperton transform show that crust at the eastern intersection high (see Fig. 3.1b) is approx. 1 km thicker than along the transform valley, thicker even than that formed along the spreading segment to the south (Barth, 1994). At fast-spreading ridges, it has been suggested that dykes propagating along the ridge axis penetrate past the transform fault into the juxtaposed old oceanic crust, curving in the direction of the transform, and locally increasing the crustal thickness (Gregg et al., 2007, Barth, 1994). At these ridges, gravity field anomalies imply that transform systems can have crustal thicknesses that even exceed the mean crustal thickness of the spreading segment (Gregg et al., 2007) as the age-offset is generally less, and initial along-axis crustal thickness variations are much smaller (Lin and Morgan, 1992). Unlike the pattern of transform valley deepening, which is observed to depend on the age-offset of the system (Fig. 3.2d), observed seafloor shallowing across an RTI seems to be independent of spreading rate (Fig. 3.2b), with possibly a slight increase at ultra-slow spreading rates (Fig 3.1e, 3.1f). Episodic transform-crossing accretion consequently appears, therefore, to be a feature common to all RTIs, implying widespread magmatic activity at this stage of their evolution. The seafloor bathymetry only highlights the component of second-phase volcanism that is extruded on the seafloor, additional material may also be intrusively added to pre-existing crust and lithosphere across an RTI.

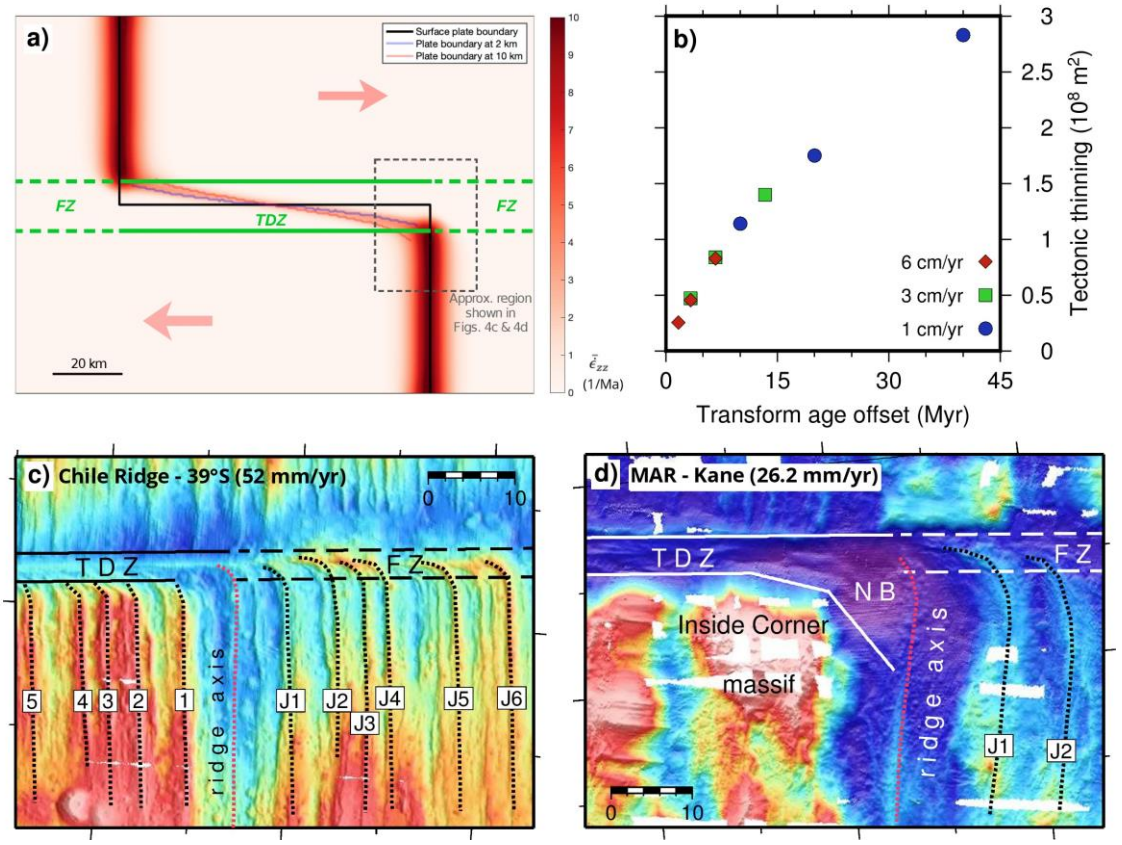

Fig. 3.4 a) Simplified plan view of mean vertical strain rates within the top 6 km for the Clipperton-like model run shown in Fig. 3. Super-imposed are the surface plate boundary (black), the increasingly oblique plate boundaries at 2 km and 10 km depth, and annotations for what we refer to Fracture Zone (FZ) and Transform Deformation Zone (TDZ). (b) Predicted transform extension $\int(\beta-1)d\perp$ for all model runs calculated in the ridge-parallel direction outside the brittle deformation zone (see Fig. 3). Transform extension scales in a simple way with age-offset similar to the change in valley depth with age-offset as shown in Fig. 2d. (c) Eastern RTI of a transform fault offsetting the Chile Rise at 39°S, individual most prominent magmatic ridges are numbered on both sides of the present-day axis. On the OC these ridges (J1-J6) extend into the fracture zone, on the IC the ridges (1-5) terminate at the southern boundary of the TDZ; d) eastern RTI of the Kane transform fault at the Mid-Atlantic Ridge. Magma-starved extension in the IC leads to formation of a massif comprising an IC core complex, the equivalent OC shows J-shaped ridges (J1, J2) extending into the fracture zone; NB: nodal basin (from Grevemeyer et al., 2021).

Bathymetric evidence for the J-shaped ridges is much more frequently preserved on the outside corner (OC) of the RTI than on the inside corner (IC) (Fig. 3.4c, 3.4d). This suggests that, analogous to the 'dueling' ridge tips at overlapping spreading centres (Macdonald and Fox, 1993), magmatically less robust spreading episodes lead to the birth of a new axial volcanic ridge between the IC and the previously active J-shaped ridge, that preferentially transfers the magmatically accreted crust to the OC, and leaves the less-active phase of 'magmatically starved' crust formed at the IC to be carried along the active transform fault. Confirmation of this scenario comes from the asymmetric distribution of dominant lithologies at segment ends: at ICs, along the transform valley and within the TDZ at slow-spreading ridges, lower crustal and upper mantle rocks are often exposed (Karson and Dick, 1984; Tucholke and Lin, 1994, Fox et al.,

1984), while OCs, including fracture zone regions, show dominantly fossil J-shaped ridges and basaltic rocks (Karson and Dick, 1984).

The observations summarized here imply that transform lithosphere is formed in two distinct phases, contradicting the current model that transforms represent conservative plate boundaries. This involves three distinct processes: (i) asymmetric crustal production at RTIs leads to the formation of magmatically starved inside-corner crust, and outside-corner crust that often preserves axial volcanic structures in the form of J-shaped ridges; (ii) the inside-corner crust is then subject to transform-perpendicular extension and thinning as it passes along the transform, deepening the transform valley; (iii) finally this extended and thinned former inside-corner crust is covered and possibly intruded by magmas from the opposing ridge as it passes the second RTI. Evidence from our global study indicates that these two phases of accretion separated by a period of transform extension occur at all spreading rates. Therefore, the formation of oceanic crust near transform faults differs fundamentally from elsewhere along the spreading system.

3.1.2 Oceanographer Transform Fault

The Mid-Atlantic Ridge is highly segmented and offset by a large number of transform faults. The most prominent offsets occur in the equatorial Atlantic with the Chain, Romanche and St. Paul transform systems. In contrast to the large equatorial OTFs showing a large degree of complexity (e.g., Searle et al., 1994; Ligi et al., 2002) represents the 120 km offset Oceanographer transform fault to the south of Azores near 35°N a type-example of an OTF along the slow spreading MAR. Swath-bathymetric data collected about 20 years ago (Rabain et al., 2001) showed that the transform fault runs within a ~10 km wide valley and has two well-defined segments which are linked by a small pressure ridge roughly at the centre of the OTF system. The age-offset of the OTF is about 11 Mio. years (Cormier & Sloan, 2019) and hence spreading at 22 mm/yr.

The global Centroid-Moment-Tensor catalogue of Columbia University, New York, reports 9 earthquakes larger than M>5.6 (since 1976) and five earthquakes with M>6 in 1982, 1990. 2003, 2010 and 2019 (i.e., roughly one event M>6 every 10 years). Excluding the large offset OTF in the equatorial Atlantic, it is world-wide the OTF with the largest moment release of any transform fault with offset <400 km.

Seismic data obtained along the Oceanographer (Ambos & Hussong, 1986) suggests that crust sampled along the transform valley is only slightly thinner (4-5 km) compared to normal (6-7 km) oceanic crust (e.g., Grevemeyer et al., 2018). However, the velocity structure seems to be different, providing several percent slower values in the lower crust, which may suggest that magmatic crust has been overprinted from faulting and fracturing and hence would support high porosities as deduced for the Gofar OTF in the Pacific (Roland et al., 2012).

Two micro-seismicity surveys were conducted at the Oceanographer OTF near its eastern intersection with the Mid-Atlantic Ridge in 1974 and 1980 (Rowlett, 1981; Cessaro and Hussong, 1986). Both studies revealed similar patterns, suggesting that micro-seismicity did not follow the right-angular geometry of an RTI as sketched by plate tectonics (e.g., Wilson, 1965), but revealed that micro-earthquakes “cover a broad swath across the corner of the intersection zone” (Cessaro and Hussong, 1986). Further, Cessaro and Hussong (1986) did not observe the expected strike-slip deformation, but rather found that the area was under extension. Matching patterns were observed in dives of the submersible Alvin, revealing on the transform walls

inward facing scarps and terraces supporting extension across the transform at the walls (Fox et al., 1985). Further, the tectonic deformation zone along the transform valley seems to be "confined to a narrow swath (…) that is centred along the axis of maximum depth" (Fox et al. 1985).

3.2 Aims of the Cruise

The cruise M170 aimed to test constraints derived from an extensive study of OTF (Grevemeyer et al., 2021), which was introduced above, conducting a case study at the Oceanographer transform fault offsetting the Mid-Atlantic Ridge at 35°N (see. Fig. 3.5).

Global observations suggest that transform valleys are always much deeper than the associated fracture zones (Fig. 3.1 and Fig 3.2a), suggesting that transform valleys are buried before being converted to fracture zones. The burial of the transform valleys is supposed to be related to a second phase of magmatic activity as the plate moves along the RTI (ridge-transform-intersection), which can readily be identified in seafloor imagery and seafloor geology. However, high-resolution data supporting active magmatic activity at RTIs are generally lacking as most existing data were acquired 20 to 40 years ago and detailed sampling of transform systems has not been carried out since the 1980s (e.g., Kason and Dick, 1983; Gallo et al., 1985). Therefore, a major goal was to provide new observational high-resolution evidence from the Oceanographer (and Hayes) transform faults to support the idea pushed by our previous work (Grevemeyer et al., 2021) and hence conducted detailed swath-mapping surveys of the RTIs. In addition, geological sampling was used to associate characteristic bathymetric features with rocks dredged from the seafloor.

Further, the compilation of bathymetric data found evidence for a very deep transform valley that tend to get deep as spreading rate decreases (e.g., Fig. 3.2c). Numerical modelling indicates that brittle and ductile flow driven by a kinematic orthogonal strike-slip surface boundary condition will rapidly transition into an oblique extensional shear zone at depth. This extension supports the development of deep transform valleys. Thus, the extension shall be reflected in the stress field along any transform fault, which can be revealed by focal mechanisms of micro-earthquakes along a transform offset. Therefore, a large network of ocean-bottom-seismometers (OBS) and hydrophones (OBH) was installed to reveal high resolution hypocentral parameters of local micro-earthquakes. This approach, however, was only a pilot-study to reveal the rate of seismicity along the Oceanographer transform fault and define the most active features of the fault (e.g., surface trace of the transform fault, RTI, walls of the transform fault), providing guidance of a future long-term deployment.

3.3 Agenda of the Cruise

The cruise was conducted under Corona restrictions at the height of the third wave of the Corona pandemic in Europe and is a pilot study to provide new observational evidence for processes shaping transform faults, focusing on bathymetric mapping, deployment and recovery of a network of OBS/H to reveal seismicity patterns and sampling the seafloor. Main features of the programme were:

1. Swath-mapping (EM122 survey) to reveal the detail structure of the 120 km long Oceanographer transform fault, addressing questions like: Does the Oceanographer (and Hayes)

OTF also display characteristic J-shaped volcanic ridges, which are abundant in the global record primary at faster spreading rates? Are all RTIs characterized by magmatic activity? Can we observe a time-dependent variability of accretion by mapping the near ridge fracture zone valleys? *Please note that during the cruise bad weather conditions forced us to leave the Oceanographer, at the same time offering the chance to obtain data from a second major ridge offset – the Hayes transform fault roughly 150 km further south.*

2. 10-days micro-earthquake survey along the Oceanographer transform with in total 29 OBS/H stations to reveal depth distribution of micro-earthquakes and their relationship to the fabric of the transform. Focal mechanism shall reveal the stress field and if the OTF is under extension.

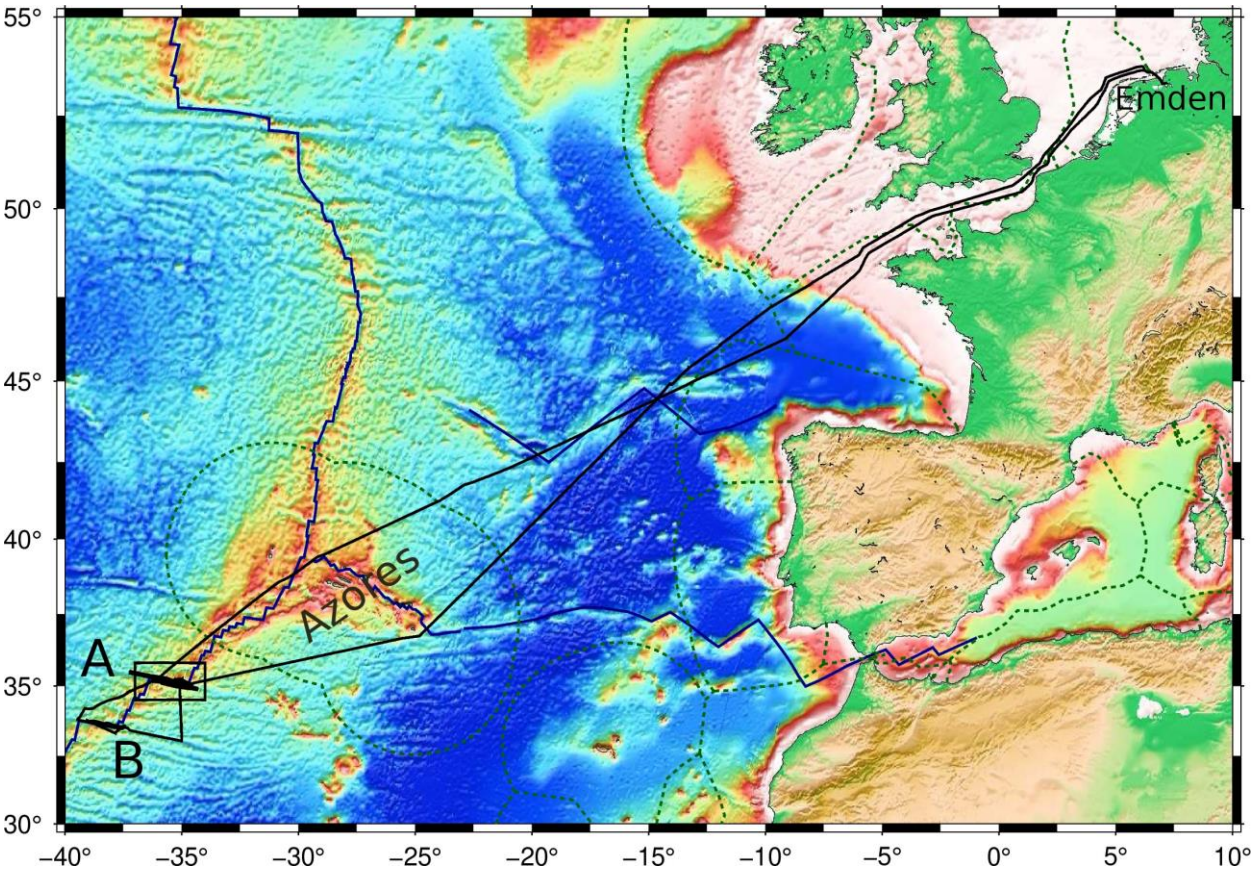

Fig. 3.5 Track chart of R/V METEOR Cruise M170. Bathymetry from Smith and Sandwell (1997). Two main working areas (Oceanographer and Hayes Transform Faults, Working Areas A+B, respectively. Territorial waters are marked by broken-lines.

3. Characterizing the strike of seafloor fabric in the transform fault and at the RTIs using side-scan sonar imagery, studying tectonic features where stresses should rotate by 90° from an extensional ridge crest setting to a strike-slip fault. *Please note that both technical issues and bad weather conditions caused us to abandon this effort and hence no side-scan sonar images were obtained.*

4. Characterizing magmatic activity at the adjacent spreading segments, at the RTI and at the inside (IC) and outside corner (OC) of the RTI using video footage. *Please note that bad weather conditions caused us to abandon this effort and hence neither video coverage nor photo images were obtained.*

5. Characterizing the lithology at RTI, IC and OC and along the fracture zone using dredging.

6. Revealing hydrothermal activity using the video observations and MAPR deployed with the video system and the side-scan sonar. *Please note that deployment of MAPR was planned to be run during either side-scan sonar or mini-OFOS deployment and therefore the number of data is rather limited.*

4 Narrative of the Cruise

On 11th of January 2021 METEOR left its berth in Emden at 7:30 UTC, tackling its expedition M170 to survey the Oceanographer Transform Fault, a major 120 km long offset of the Mid-Atlantic Ridge to the south of the Azores.

Just 40 min after it left the cay, the vessel reached the harbour's log; at 9:30 METEOR sailed along the river Ems and left the mouth of the Ems at noon. Strong head winds and current and waves of ~3-4 m reduced the speed of the vessel, dropping below 8 kn for roughly 10 hours while heading westwards. Fortunately, conditions became better while sailing farther west and METEOR could keep a transit pace of approx. 11-12 kn for most of the time while sailing through the North Sea and English Channel, passing Dover on 12th January at ~4 p.m. and leaving the English Channel at 8 p.m. of the 13th, steaming south-westwards towards Azores at ~10-11 kn and south-westerly winds and waves of 2-3 m. On 14th of January, METEOR left the national waters of France and underway data, including swath-mapping bathymetry using the shipboard Kongsberg EM122 echosounder, were collected.

Weather prediction along the planned transit into the working area were expected to worsen. Therefore, it was decided, based on advice of the German Meteorological Service (DWD), to choose a longer and more easterly route. However, better predicted sea conditions allowed to keep a faster transit speed of ~10 kn instead of facing strongly reduced speed and high waves to the north of Azores while passing through a fierce low-pressure area. Additionally, the calmer sea to the east of the storm allowed the preparation of seismic equipment on the deck of METEOR. On 15th and 16th of January, METEOR stopped three times to lower during 3 casts the release units of the ocean-bottom-seismometers to 1000 m, testing their functionality. On Sunday 17th of January, we entered at 3:35 p.m. the territorial waters of Portugal/Azores and suspended collection of underway data. We left the exclusive economic zone of Azores on 19th at 6 p.m. and reached the working area on 20th of January, conducting a XBT station at 15:15 a.m. to collect a sound velocity profile for the swath-mapping system, converting measured travel times of the EM122 echosounder into water depth. At 17:12 p.m., OBS01 was the first ocean-bottom-station to be deployed near the eastern ridge-transform intersection. 16 hours later, the 27th OBS was deployed at the western ridge-transform intersection, providing full coverage of the Oceanographer Transform fault. Thereafter, we sailed back to the east, mapping the seafloor to the north of the transform fault before deploying two additional ocean-bottom-hydrophones on the inside corner high at the eastern RTI.

Two hours late, at ~8 p.m. UTC on 21st of January the side scan sonar was deployed in the fracture zone roughly 20 nm east of the RTI. Unfortunately, at 3500 m water depth and hence before obtaining any data, we observed a malfunction of the system and had to recover the deep-tow system. Later, we detected that a cable was damaged. We therefore decided to run a

bathymetric mapping survey along the active transform fault. On the 22nd of January the mapping was suspended to conduct a side scan sonar survey in the vicinity of the western RTI. Unfortunately, the communication with the side scan failed immediately after it was deployed. We therefore recovered the tow-fish of the side scan sonar and steamed farther west, mapping a ~60 km long portion of the western branch of the fracture zone. Returning to the east, we mapped the seafloor adjacent to the fracture zone and transform fault.

In the evening of the 23rd of January, we conducted the first geological station, deploying a dredge at 23 UTC on a patch of high backscatter intensity of the EM122 swath-mapping system at the toe of the southern wall of the eastern branch of the fracture zone. The dredge returned serpentinzed mantle rocks. In total, 8 additional sites were dredged in the outside corner domain of the eastern RTI and only one dredge was empty. The most common rock type were basalts.

On Monday 25th of January, we had to abandon the dredge programme as strong wind and sea with 5-6 m caused fierce rolling of the ship. Farther south conditions were expected to be better and METEOR sailed therefore roughly 140 nm southwards. Strong headwinds and waves forced us to reduce the speed. On 27th of January we reached the fracture zone trace of the Hayes transform fault and sailed eastward, collecting EM122 swath mapping data of good to very good quality along the Hayes transform / fracture zone system. We mapped the western fracture zone, the transform fault and the eastern fracture zone out to ~50 km from the ridge-transform intersection (RTI) on either side. Thereafter, we returned in the small hours of the 29th back to the western RTI to dredge at five different sites. Unfortunately, even in the south the weather conditions got worse and we had to cancel three of the five planned dredges. We therefore continued to map the eastern fracture zone of Hayes before sailing on the 30th of January back north to recover the ocean-bottom-seismic stations. We reached the first OBH at 9 a.m. on 31st of January and released it. Unfortunately, weather conditions were still rough and strong wind. Consequently, weather conditions slowed down the recovery. Over the next 10 hours we covered in total 6 OBH and suspended recovery during the night and conducted a short mapping campaign to close gaps in the bathymetric coverage of the Oceanographer transform.

In the early evening the tragic death of one of the crew members was detected; he was found dead in his room. Therefore, the captain decided to end the cruise as soon as possible. However, 5 OBH would release automatically on 4th of February and return to the surface. Those 5 OBH had to be recovered the next day to prevent losing the stations and data recorded during the last 10 days. Recovery began at 9 a.m. UTC and was again slowed down by bad weather. At 7 p.m. UTC of 1st of February 2021 the last of the 5 OBH was recovered and METEOR left the working area, sailing back northward. Unfortunately, 18 OBS (with automatic releases programmed for summer 2022) remained on the seafloor to be recovered as soon as possible during another cruise.

During the transit towards Emden seafloor depth was mapped using the EM122 echosounder. Of course, mapping was suspended in territorial waters of Portugal/Azores and all scientific measurements were stopped on 6th of February 2021 at 11:30 UTC while entering the Spanish waters. We entered the English Channel in the early morning of 8th of February and reached the pilot at the mouth of the river Ems on 10th of February 2021 at 8 a.m. Four hours later, METEOR reached the lock and was back in port.

5 Preliminary Results

5.1 Swath mapping - EM122 Kongsberg echosounder

The RV METEOR is fitted with a Kongsberg EM122 1°x2° multi-beam deep ocean echosounder, with two transducer arrays fixed to the ship's hull operating at 12 kHz. Data acquisition is based on successive transmit-receive cycles of this signal. The transmit beam is 150° wide across-track and 1° along-track direction. The system has 432 beams, sampling seafloor depth at high resolution. The beam spacing can be defined as equidistant or equiangular, and the maximum seafloor coverage fixed or adjusted according to seabed and weather conditions. Seabed depth and reflectivity are recorded against UTC and GPS location. The raw depth data are processed to obtain depth contour maps, and the acoustic amplitude processed to obtain backscatter amplitudes. Swath bathymetry and backscatter data were acquired within the survey area at the Oceanographer and Hayes transform faults and fracture zones and during transit in international waters (see Fig. 3.5).

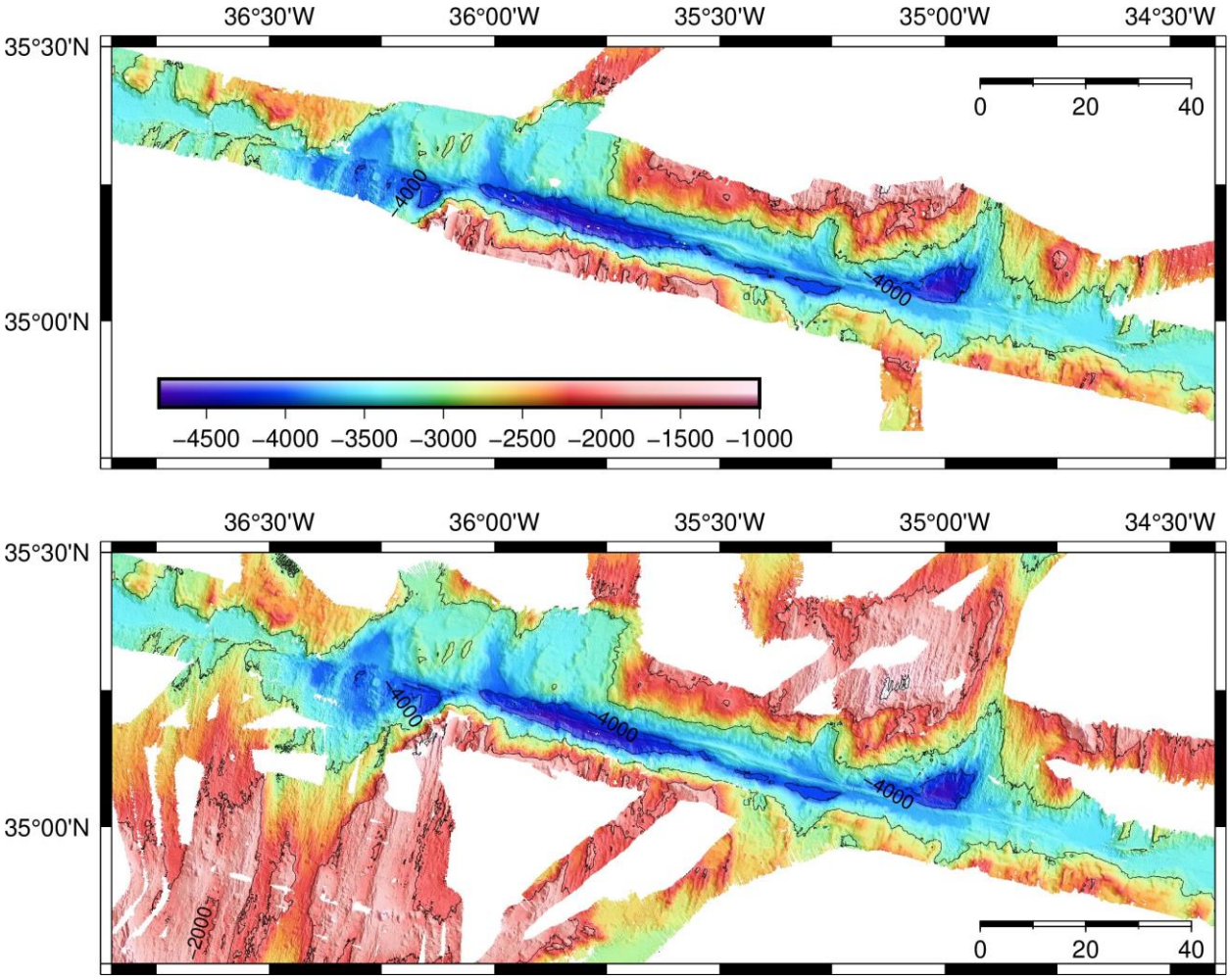

Fig. 5.1 (Top) Bathymetric coverage of the Oceanographer transform fault from M170. (Bottom) M170 EM122 data (except transits in and out of the working area) merged with data of opportunity from US American NOAA archive and the German BSH archive.

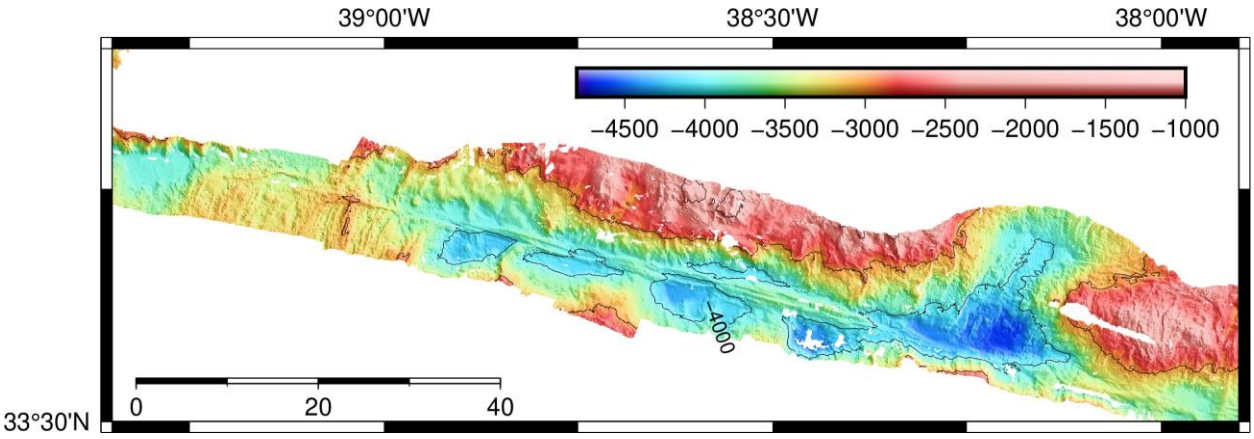

Fig. 5.2 Bathymetric EM122 data of M170 from the Hayes Transform Fault.

During the cruise bathymetric data were cleaned, editing raw swath data either with MB-System or with CARAIBES Software. Tests about the resolution of the EM122 revealed that bathymetric grids with a footprint of 50 m could be obtained. Fig. 5.1a shows the coverage and seafloor morphology at the Oceanographer OTF and Fig. 5.1.b has the same area with tracks of opportunity from the BSH archive and the NOAA archive added to the M170 data. In Fig. 5.2 we present the bathymetric map of the Hayes OTF and Fig. 5.3 focuses on the western RTI of the Hayes, providing both bathymetry and backscatter intensity, providing an assessment of bright and hence young rocks.

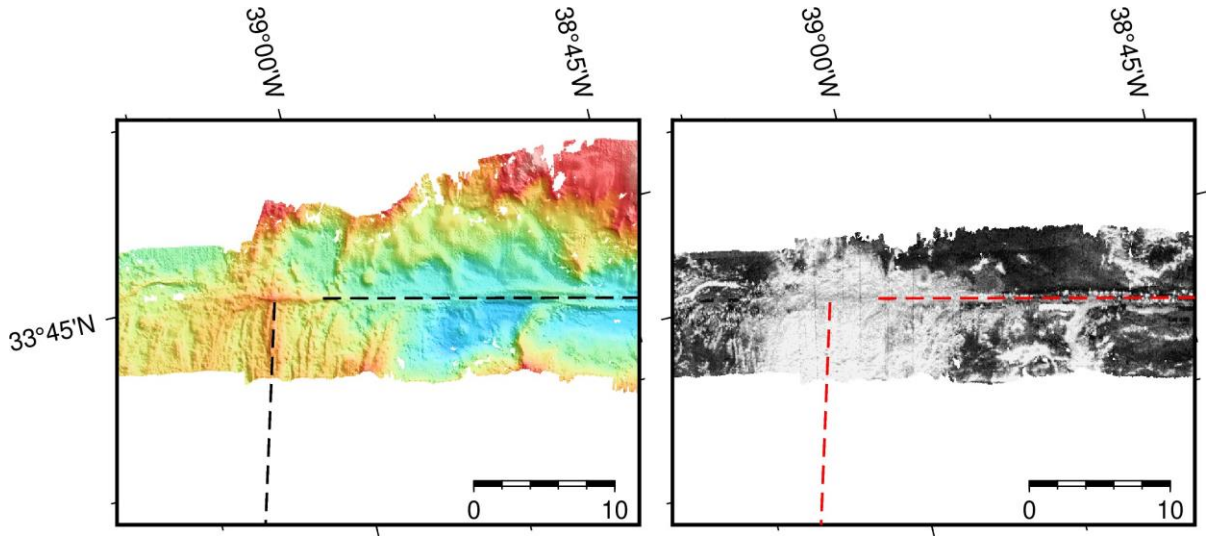

Fig. 5.3 (Left) EM122 bathymetry and (Right) backscatter data of M170 from the Hayes Transform Fault.

Grevemeyer et a. (2021) had found that transform valleys are always deeper than the associated fracture zone, even though seafloor age increases. In general, cooling of the lithosphere causes older seafloor to subside with age. Both data from the Oceanographer and Hayes OFT support the very same pattern. Bathymetry of both RTIs of the Oceanographer OTF show a shallowing of the seafloor while moving from the active transform fault into the inactive fracture zone, but backscatter data are not providing bright areas revealing young volcanism, suggesting that today tectonic processes dominate the system. However, the western intersection of the Hayes OTF with the Mid-Atlantic Ridge displays strong evidence of recent magmatic

activity and J-shaped volcanic ridges, including a very bright seafloor reflectivity, supporting young volcanism. Most interestingly, the bright reflectivity extends well onto the older plate (forming a so called "rooster comb"; e.g., Gallo et al., 1986; Barth et al., 1994), suggesting plate boundary cutting magmatism. Further, the fracture zones provide some evidence for J-shaped ridges both at Oceanographer and Hayes OTF and thus support that repeated magmatic phases occurred frequently in the past.

5.2 Micro-seismicity survey at the Oceanographer Transform Fault

The seismological network was operated between 21st of January to 31st of January 2021, monitoring seismicity along the Oceanographer Transform Fault. The network consisted of 6 Trillium Compact OBS, 12 short-period (4.5 Hz geophone) OBS and 11 OBH (Fig. 5.4) of GEOMAR'S OBS pool. Please note that after an incident on 31th of January it was decided to leave the study area earlier and to recover only those stations that would automatically surface on 4th of February 2021. Due to the bad weather conditions and predictions, we had decided to use for all OBS releases time on 1st of July 2022, giving us more flexibility in case that another low-pressure system would affect the working area, hindering a recovery. Therefore, preliminary results reported here are only based on data recorded at the 11 OBH instead of being based on the entire network of 29 OBS/H. We like to note that all OBS, except one, were recovered in June of 2021 during the cruise M175 of RV METEOR.

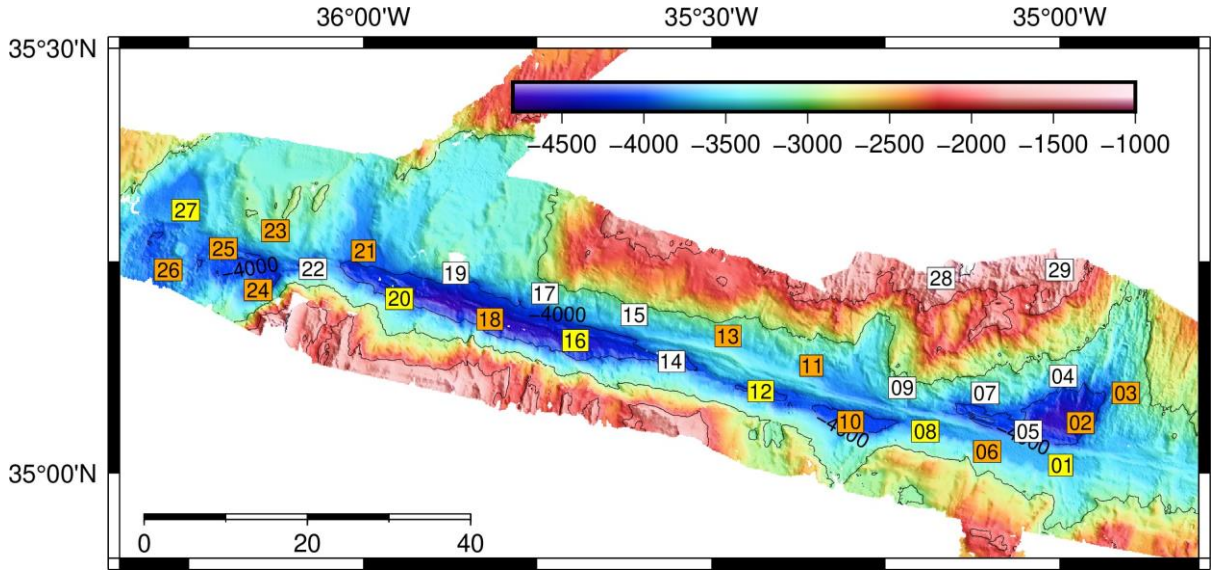

Fig. 5.4 Layout of the seismic network. Seismic stations are numbered squares, colour indicates instrument type; white OBS; orange: short-period OBS; yellow: broadband OBS.

Raw data recorded on the OBH were converted to Pseudo-segy (or PASSCAL-segy) format of IRIS and to obtain more manageable files sizes and for applying time corrections files were cut into 24 hours records.

Hydrophone data are generally much more affected by ocean noise than seismometer data. For an initial assessment of seismicity pattern, we therefore scanned records by eye instead of applying a standard and automatic triggering approach (e.g., Grevemeyer et al., 2013; 2019). After defining seismic events, files were cut and stored into event-based subdirectories. We cut

local earthquakes into a time window length of 3 minutes, starting 30 s prior to trigger/event time. The SEGY traces in the event directories are converted first into SAC, and then into MiniSEED waveform format, which makes it possible to store all traces associated with an event into a single waveform file. After conversion, data are registered into the SEISAN database (Havskov and Ottemöller, 2005). P-wave onset times of local earthquakes are hand-picked and events were located with the HYPO earthquake location procedure of the SEISAN package. An example of an event is shown in Fig. 5.5. Travel times were calculated using a 1-D velocity model used to record micro-earthquakes at the Logatchev core complex at the Mid-Atlantic Ridge (Grevemeyer et al., 2013). For this report, we preliminary locate 110 of the about 150 events recognized in the daily files and thus found an event rate of 10-15 local earthquakes per day.

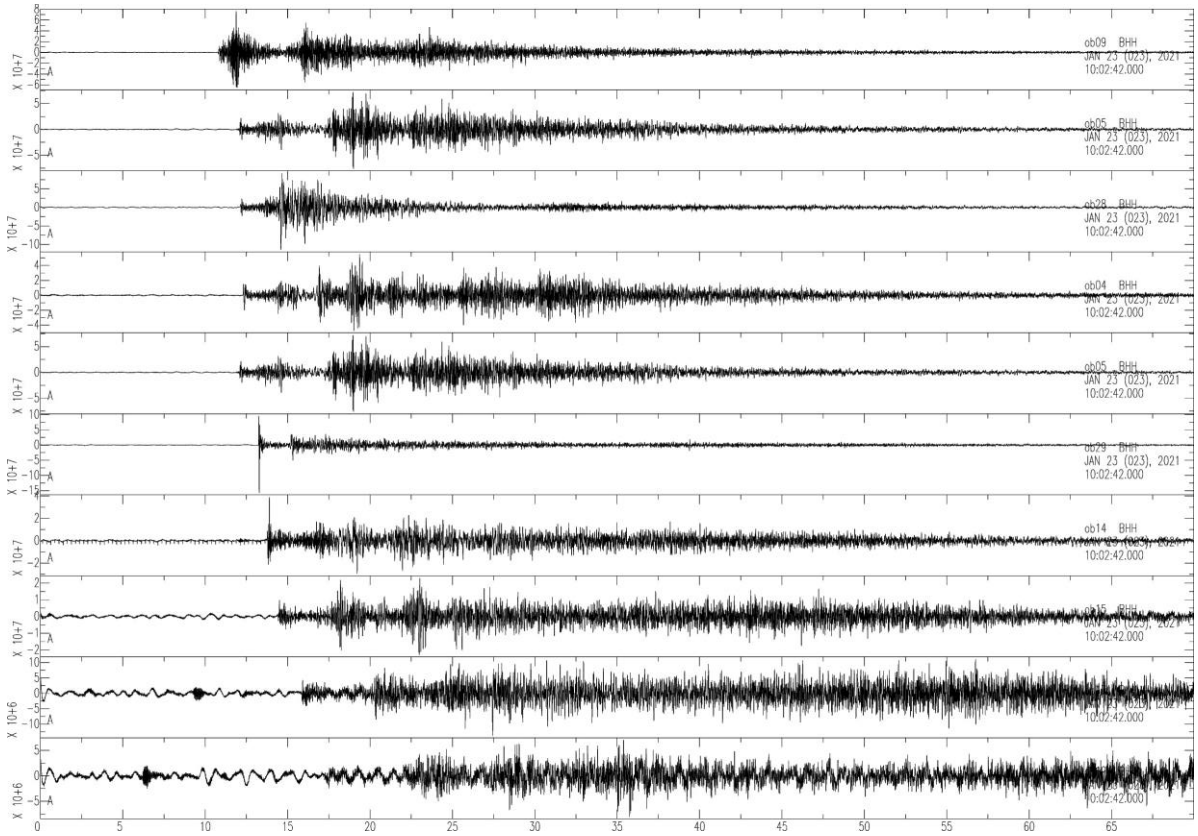

Fig. 5.5 Local earthquake recorded on the hydrophone channels on 21st of January 2021 at 10:02:42

The preliminary analysis reveals that the eastern inside corner of the ridge-transform intersection is a major hotspot of seismic activity (Fig. 5.6). However, please note that the eastern RTI had the best coverage by OBHs (white numbered squares in Fig. 5.4 & 5.6), while the coverage with OBH was much poorer elsewhere along the transform fault. Further, additional activity occurred along the surface trace of the transform fault, while the walls of the transform were seismically inactive, at least away from the RTI.s We expect that the number of local earthquakes and quality of the location procedure will increase when the data from all stations are available after their recovery during M175.

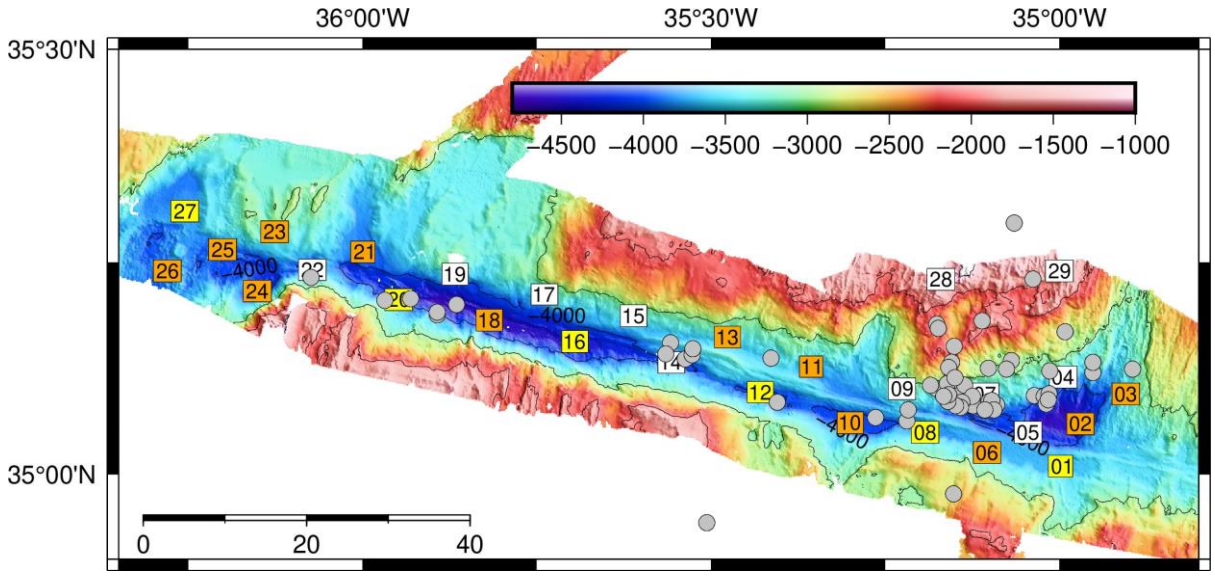

Fig. 5.6 Seismic events (grey dots) recorded at OBHs only (OBH are marked by white numbered squares).

5.3 Dredge samples from the Oceanographer Transform Fault and Fracture Zone

Igneous and sedimentary samples were taken by a chain bag dredge. Station locations were chosen based on the bathymetry and backscatter data. The dredge tracks were located mostly on steep slopes and high backscatter intensity areas to avoid thick sediment cover. In total, twelve dredges were performed recovering a total of 43 rock samples. Ten of these dredges were located at the Oceanographer OTF and two at the Hayes OTF. Fig. 5.7 shows an overview of the dredge locations at the Oceanographer OTF and Fig. 5.8 shows the locations at Hayes OTF.

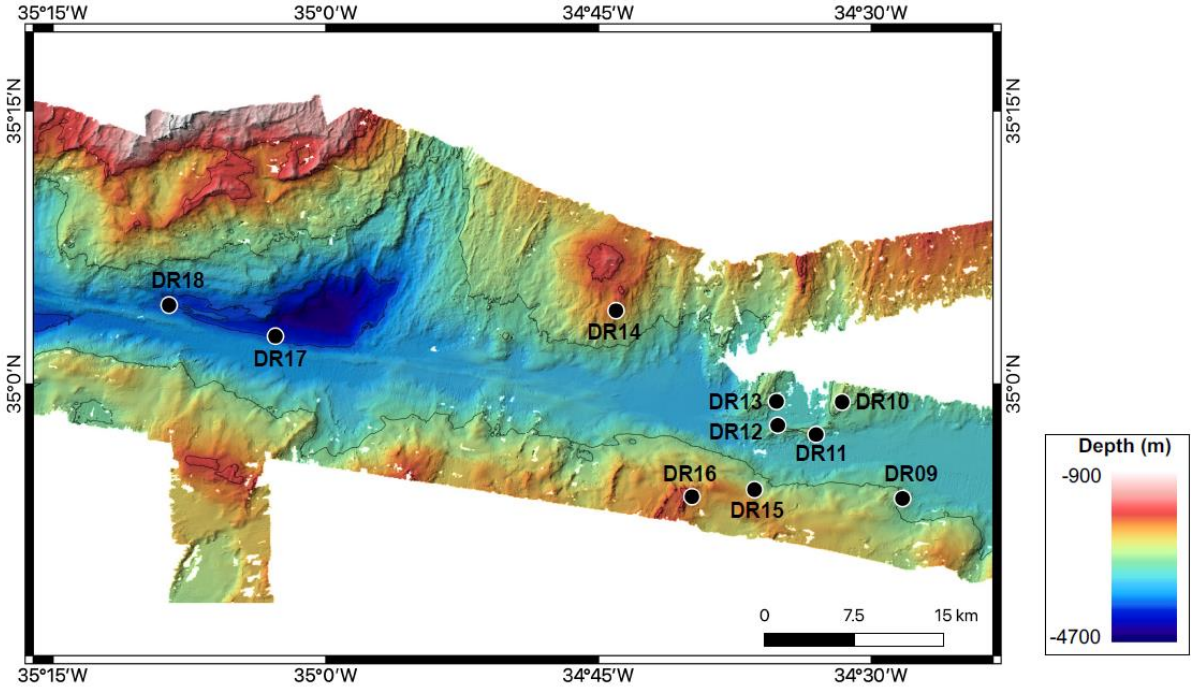

Fig. 5.7 Dredge sites at the eastern RTI of the Oceanographer OTF and adjacent fracture zone.

The main goal of the rock sampling at the Oceanographer OTF was to sample a transform system in detail, to identify the different lithologies and to get a better understanding about the magmatic processes at transform faults. The Oceanographer OTF was sampled by 10 dredge stations of which 7 retrieved rocks. The inside corner/fracture zone was sampled by 3 dredges (DR09, 15, 16) which contained mostly peridotites, gabbros and a small amount of basalt in one dredge (DR16). The outside corner was sampled by five dredges retrieving mostly basalts and some carbonates. Dredges 17 and 18 were located within the transform fault and did not retrieve any rocks.

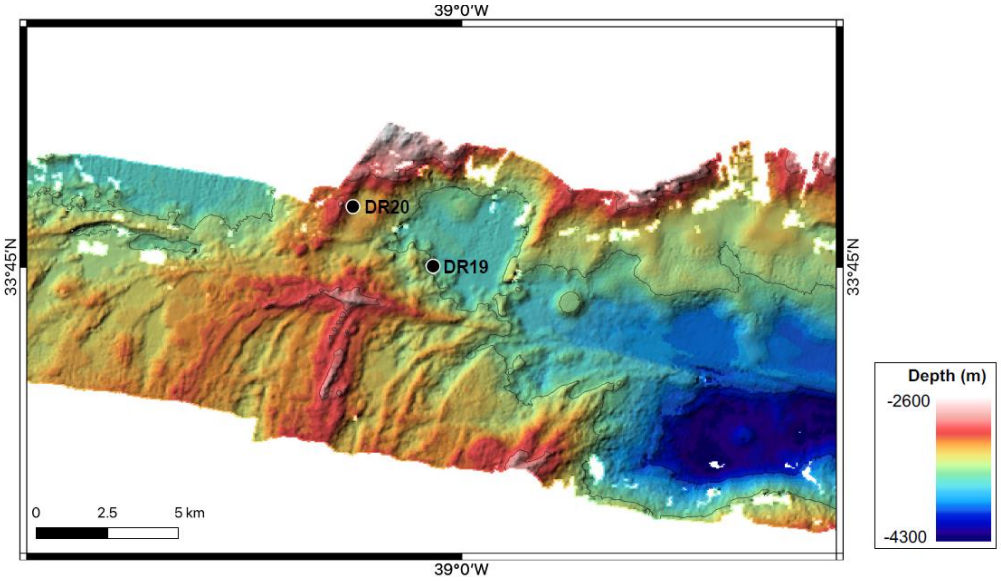

Fig. 5.8 Dredge sites at the western RTI of the Hayes OTF at the prominent "rooster comb".

The objective of the sampling along the RTI of the Hayes OFT was to find young magmatism on the older plate passing the ridge axis. Hayes OTF was sampled by 2 dredge stations (DR19, 20). These two dredges were located on the older plate, on the rooster comb and hence on the older plate, which has a very bright seafloor reflectivity (Fig. 5.3). These two dredges recovered the freshest basalts of the expedition basalts.

On board the samples were described and packed for petrological and geochemical analyses.

The samples recovered during M170 can be grouped into different lithologies: peridotite, gabbro, basalts and sedimentary rocks. We refer to the M175 cruise for further details on extended rock sampling and lithology at the Oceanographer Transform Fault.

5.4 Instruments suffering from bad weather conditions

During M170 a number of different instruments were originally planned to be used to study the nature of the seafloor. Unfortunately, after entering the study area, while weather conditions were still fair, we had some technical issues with the EDGTECH side-scan sonar. Later, after the technical issues were solved, the sea state got too rough and therefore the side-scan sonar could not be deployed again.

Further, we had planned to obtain video and photo coverage of RTIs, searching for evidence of recent magmatic activity. However, GEOMAR's Mini-OFOS requires good

conditions with little ocean waves and swell. Unfortunately, the rough sea state of 4-6 m during most of the survey prevented us to obtain any photo or video coverage.

In addition, hydrothermal plume imaging was related to either side-scan sonar or OFOS deployments using so called MARPs. They should have been attached to the cable of the deep-tow systems, scanning at the same time for hydrothermal plumes. Therefore, the deployment of the MARP was limited to the two side-scan sonar deployments which were abandoned after the side-scan failed and hence no hydrothermal activity was detected.

6 Ship's Meteorological Station

(A. Raeke)

RV METEOR left the port of Emden in the morning of 11.01.2021. At the beginning of the voyage, the sailing area was influenced by a high over southern Germany and a storm low over the northern North Sea, experiencing a strong to stormy westerly moist current. With strong headwinds around 7 Bft and seas with swells of 3m, RV METEOR initially had difficulties to progress towards the English Channel. In the following days, the storm low relocated to southern Scandinavia. In the evening of 12.01. an associated trough crossed the Strait of Dover. After a short time of abating, on the morning of the 13.01. the wind in the English Channel picked up again, reaching 6 to 7 Bft, shifting from north to west. The sea reached only a height of 2.5m. On the night of 14.01. while exiting the English Channel a cold front of a low-pressure system crossed with further showers and wind of strength 6 to 7 Bft. In the following days a high-pressure system over Spain extended to Madeira until 17.01. At the same time, a storm low approached from the west, resulting in a stormy southwesterly flow. As on the direct route to the south-of the Azores working area significant wave heights of 5 to 6m were expected, the transit route was moved further east and to the south of the Azores. It was adjusted daily according to the weather forecasts. Nevertheless, RV METEOR battled a southwesterly headwind of 5 to 6 Bft and significant seas of 2 to 3m south of the Azores until Jan. 18. The region was crossed from an associated trough from an Ireland low., the wind briefly turned from SW to NW. On Wednesday, January 20, while reaching the research area a frontal system of a storm low near Newfoundland crossed the working area with showers. This was accompanied by a southwesterly wind with force of 5 to 6 Bft and a significant sea of 3 m with a swell from northwest to west. On 21.01. within a high pressure ridge the weather eased for a while with winds around 4 Bft or even less. From Friday, 22.01., Atlantic frontal systems rapidly crossed the working area. The usual Azores high pressure shifted to Madeira persisting almost stable until 02.02. Southwesterly winds of 6 to 7 Bft with significant seas of 3 to 4m were generated between the high and lows over the North Atlantic. Sunny periods changed with rain at times, or local showers, associated with local thunderstorms. From the 25.01., a high swell from various directions developed on the edge of the storm low causing a high cross sea. The strong air pressure difference was reflected in the wind with force 7 Bft and gusts of up to 10 Bft on Tuesday 26.01. The significant sea rose to 4m with the swell mostly from west to northwest. It was mostly cloudy with rain or showers with isolated thunderstorms. The work with the dredge was increasingly hampered. Therefore, it was decided to continue the work in a more southern area of the Mid-Atlantic Ridge in order to avoid a storm low expected near the original working area on Thursday. On Wednesday/Thursday (Jan. 27.01./28.01.) on transit to the south a southwesterly wind of 6 to 8 Bft blew and significant seas increased to 4 to 6m. However, even

in that area, only a few deployments could be completed with the dredge due to only marginally better conditions of wind and significant sea. Thus, on Friday/Saturday (29.01./30.01) along a west/east profile, survey work took place in somewhat calmer waters with a significant sea of 3 to 4m and a southwesterly wind of force 6 Bft. In the meantime, a hurricane force low (968 hPa) at 47°N 029°W moved towards Ireland and a severe storm low (960 hPa) at 36°N 061°W followed on 30.01. (958 hPa 44°N 046°W). At the same time an almost stationary high (1022 hPa) was located near Madeira with a ridge extending over the Azores and further to the northwest. Between these pressure areas, a strong southerly to southwesterly wind blew with intermittent squalls and seas of 4 to 6 m. The swell came from the northwest with a second one from the west. Due to the cross sea, the transit to the original working area started on Jan 30. and the recovery of the seismometers started in the morning of Jan 31. The research area was located prefrontal of a severe storm low, associated troughs crossed with showers/thunderstorms on Monday 01. February. On the rear side the wind shifted west to northwest around 6 Bft. Due to a tragic incident on board the RV METEOR finished expedition M170 and started the return trip to Emden. On 02.02. the area was crossed by a cold front of a low-pressure system near Ireland (980 hPa). On the rear side, northwesterly winds of 6 to 8 Bft set in, in the morning of 04.02. a significant sea of up to 7m and a swell from the northwest set in, the highest sea of this trip northeast of the Azores. The wind shifted north, isolated showers occurred, at times accompanied by thunderstorms. On Friday, 05.02, the Atlantic high extended a ridge over the cruising area to another strengthening high (1035 hPa) over the Norwegian Sea. Between this pressure structure and a low near Ireland, the sea and the northerly wind gradually subsided. On the weekend 06./07.02 RV METEOR moved with 12 knots towards the English Channel. Within a high pressure ridge the westerly wind decreased to 3 Bft, the sea with a northerly swell dropped to 1.5 m. Mostly cloudy conditions with isolated showers or some drizzle were experienced. On 07.02. the east to northeast wind increased temporary to 6 Bft due to the location of a low over northern France and a Scandinavian high. The significant sea reached 2.5m at the entrance and exit of the English Channel. On Monday and Tuesday, snow showers occurred in a rather strong easterly flow, the air temperature entered the permanent frost range at the exit of the Channel.

In the morning hours of 10.02. Emden was reached. The weather showed changeable cloudiness within a northeasterly wind of force 4 to 5 Bft. It was frosty cold with a temperature of minus 2 degrees

7 Station List M170

7.1 Station List of Ocean-Bottom-Seismometer and Hydrophone deployments

Station No.		Date	Gear	Time	Latitude	Longitude	Water Depth	Remarks/Recovery
METEOR	GEOMAR	2021		[UTC]	[°N]	[°W]	[m]	
M170_6-01	OBS01	20.01.	OBS	17:12	35° 00,565'	034° 59,725'	3699	recovered 10.06. / M175
M170_6_02	OBS02	20.01.	OBS	17:38	35° 03,584'	034° 58,189'	4302	recovered 10.06. / M175
M170_6_03	OBS03	20.01.	OBS	18:12	35° 05,712'	034° 54,262'	3343	Recovered 10.06. / M175
M170_6_04	OBH04	20.01.	OBH	19:00	35° 06,895'	034° 59,670'	3473	recovered 31.01.
M170_6_05	OBH05	20.01.	OBH	19:36	35° 03,013'	035° 02,653'	4370	recovered 31.01.
M170_6_06	OBS06	20.01.	OBS	20:07	35° 01,544'	035° 06,224'	3663	recovered 10.06. / M175
M170_6_07	OBH07	20.01.	OBH	20:49	35° 05,691'	035° 06,426'	3662	recovered 31.01.
M170_6_08	OBS08	20.01.	OBS	21:32	35° 02,984'	035° 11,571'	3831	recovered 10.06. / M175
M170_6_09	OBH09	20.01.	OBH	22:05	35° 06,063'	035° 13,559'	3120	recovered 01.02.
M170_6_10	OBS10	20.01.	OBS	22:48	35° 03,613'	035° 18,023'	4023	recovered 10.06. / M175
M170_6_11	OBS11	20.01.	OBS	23:37	35° 07,589‘	035° 21,294‘	3521	recovered 10.06. / M175
M170_6_12	OBS12	21.01.	OBS	00:19	35° 05,816'	035° 25,847'	3943	recovered 10.06. / M175
M170_6_13	OBS13	21.01.	OBS	01:06	35° 09,748'	035° 28,607'	3640	recovered 10.06. / M175
M170_6_14	OBH14	21.01.	OBH	02:00	35° 07,935'	035° 33,534'	4199	recovered 01.02.
M170_6_15	OBH15	21.01.	OBH	02:36	35° 11,203'	035° 36,702'	3285	recovered 01.02
M170_6_16	OBS16	21.01.	OBS	03:09	35° 09,436'	035° 41,691'	4439	recovered 11.06. / M175
M170_6_17	OBH17	21.01.	OBH	03:45	35° 12,744'	035° 44,367'	3446	recovered 01.02.
M170_6_18	OBS18	21.01.	OBS	04:18	35° 10,917'	035° 49,085'	4582	Lost
M170_6_19	OBH19	21.01.	OBH	04:53	35° 14,163'	035° 52,045'	3481	recovered 01.02.
M170_6_20	OBS20	21.01.	OBS	05:27	35° 12,359'	035° 56,843'	4094	recovered 11.06. / M175
M170_6_21	OBS21	21.01.	OBS	06:01	35° 15,714'	035° 59,787'	3893	recovered 11.06. / M175
M170_6_22	OBH22	21.01.	OBH	06:38	35° 14,462'	036° 04,304'	3754	recovered 01.02.
M170_6_23	OBS23	21.01.	OBS	07:14	35° 17,142'	036° 07,542'	3196	recovered 11.06. / M175
M170_6_24	OBS24	21.01.	OBS	07:51	35° 12,940'	036° 09,048'	4130	recovered 11.06. / M175
M170_6_25	OBS25	21.01.	OBS	0827:	35° 15,908'	036° 12,048'	3947	recovered 11.06. / M175
M170_6_26	OBS26	21.01.	OBS	09:05	35° 14,406'	036° 16,781'	3841	recovered 11.06. / M175
M170_6_27	OBS27	21.01.	OBS	09:37	35° 18,568'	036° 15,267'	3793	recovered 11.06. / M175
M170_6_28	OBH28	21.01.	OBH	17:01	35° 13,792'	035° 10,079'	1230	recovered 31.01.
M170_6_29	OBH29	21.01.	OBH	17:49	35° 14,400'	035° 00,002'	1492	recovered 31.01.

7.2 Sample Station - List of Dredges

Station No.	Date	Time	Latitude	Longitude	Water Depth	Remarks
METEOR	2021	h	[°N]	[°W]	[m]	
M170_9 Start	23.01.	20:36	34,8953	34,4714	2984	
M170_9 End	23.01.	23:22	34,89563	34,4795	2890	
M170_10 Start	24.01.	00:34	34,9836	34,52678	2883	
M170_10 End	24.01.	03:12	34,983683	34,533217	2814	
M170_11 Start	24.01.	04:46	34,9539	34,5506	3204	
M170_11 End	24.01.	07:00	34,95518	34,55923	3214	
M170_12 Start	24.01.	07:32	34,96235	34,585783	3288	
M170_12 End	24.01.	10:29	34,9579	34,5912	3073	
M170_13 Start	24.01.	11:10	34,98418	34,5869	3086	
M170_13 End	24.01.	14:04	34,98417	34,5942	2968	empty
M170_14 Start	24.01.	15:36	35,0673	34,734	2315	
M170_14 End	24.01.	18:01	35,0673	34,74112	2150	
M170_15 Start	24.01.	19:50	34,9034	34,60705	2702	
M170_15 End	24.01.	22:26	34,8998	34,6124	2404	
M170_16 Start	24.01.	23:14	34,897	34,6644	2180	
M170_16 End	25.01.	02:47	34,8974	34,66585	2114	
M170_17 Start	25.021.	18:02	35,04392	35,04613	4065	
M170_17 End	25.01.	21:35	35,03723	35,04903	3714	empty
M170_18 Start	25.01.	22:35	35,07237	35,1436	3985	
M170_18 End	26.01.	02:00	35,0657	35,148317	4750	empty
M170_19 Start	29.01.	03:16	33,75045	39,01085	3636	
M170_19 End	29.01.	04:56	33,7504	39,0195	3414	
M170_20 Start	29.01.	06:25	33,7729	39,04115	3183	
M170_20 End	29.01.	09:12	33,7729	39,0464	3009	

8 Data and Sample Storage and Availability

Seismic data will be available after 1st of July 2022 at the PANGAEA World Data Centre, Bremerhaven (http:// http://www.pangaea.de).

Bathymetric data recorded during the survey M170 are available at the Bathymetric Data Centre of the the Bundesamt für Seeschifffahrt und Hydrographie, Rostock (http://www.bsh.de/en/Marine_data/Hydrographic_surveys_and_wreck_search/Bathymetry). Underway data (Thermosalinograph, ADCP, bathymetry) are available at PANGAEA.

Dredge samples are stored in GEOMAR's Lithothek.

Table 8.1 Overview of data availability

Type	Database	Available	Free Access	Contact
EM122	BSH	30.04.21	30.04.21	bathymetrie@bsh.de
ADCP	PANGAEA	01.07.21	01.07.21	robert.kopte@ifg.uni-kiel.de
Thermo-salino-graph	PANGAEA			mschlundt@geomar.de
Seismo-logical data	PANGAEA	30.06.22	31.12.22	igrevemeyer@geomar.de
Hard rock dredge samples	PANGAEA / GEOMAR Lithothek	01.01.22		cdevey@geomar.de

9 Acknowledgements

We acknowledge the excellent and professional sea-going operation of R/V METEOR during M170 by Captain Detlef Korte and his crew. Ship time and cruise logistics were funded by the Deutsche Forschungsgemeinschaft / German Science Foundation (DFG).

We greatly appreciate support from Captain Rainer Hammacher and the DWD discussing in December 2020 the winter weather conditions in the North Atlantic, which resulted in moving the original study area from 48°N to south of the Azores. We are very thankful that the longer transit time was compensated with additional days of ship time. Even though conditions at the Oceanographer Transform Fault were not perfect, facing 4-6 m of ocean waves and swell, the area at 48°N had up to 16 m of waves at the very same time of the January/February 2021. Moving the study area resulted into very exciting new data, opening a new avenue towards studying oceanic transform faults. Many thanks indeed for providing this unique chance during the Corona pandemic.

10 References

Abercrombie, R. E., and G. Ekström (2001), Earthquake slip on oceanic transform faults, Nature, 410, 74–77.

Ambos E.L., and D.M. Hussong (1986), Oceanographer transform fault structure compared to that of surrounding oceanic crust: results from seismic refraction analysis, J. Geodynamics, 5, 79-102.

Barth, G.A., K. A. Kastens, and E. M. Klein (1994), The origin of bathymetric highs at ridge-transform intersections: A multi-disciplinary case study at the Clipperton Fracture Zone, Mar. Geophys. Res., 16,doi:10.1007/BF01812444.

Barth, G. A. (1994), Oceanic crust thickens approaching the Clipperton Fracture Zone, Mar. Geophys. Res. 16, 51-64, doi:10.1007/BF01812445

Bird, P. (2003), An updated digital model of plate boundaries, Geochem. Geophys. Geosyst., 4, 1027, doi:10.1029/2001GC000252.

Braunmiller, J., and J. Nabelek (2008), Segmentation of the Blanco Transform Fault Zone from earthquake analysis: Complex tectonics of an oceanic transform fault, J. Geophys. Res., 113, B07108, doi:10.1029/2007JB005213.

Cessaro, R.K., and D.M. Hussong (1986), Transform seismicity at the intersection of the Oceanographer Fracture Zone and the Mid-Atlantic Ridge, J. Geophys. Res., 91, 4839-4853.

Cormier, M.-H., and H. Sloan (2019). Distinctive seafloor fabric produced near western versus eastern ridge-transform intersections of the northern Mid-Atlantic Ridge: Possible influence of ridge migration. Geochemistry, Geophysics, Geosystems, 20, 1734–1755. https://doi.org/10.1029/2018GC008101

Davis, E. E., and C. R. B. Lister (1974), Fundamentals of ridge crest topography, Earth and Planetary Sci. Letters, 21, 405-413, doi: 10.1016/0012-821X(74)90180-0.

Fox, P.J., et al. (1985), The geology of the oceanographer transform: the transform domain, Mar. Geophys. Res., 7, 329-358, doi:10.1007/BF00316773.

Fox, P. J., and D. G. Gallo (1984), A tectonic model for ridge transform ridge plate boundaries - implications for the structure of oceanic lithosphere. Tectonophysics, 104, 205–24.

Gallo, D. G., P. J. Fox, and K. C. Macdonald (1986), A Seabeam Investigation of the Clipperton Transform Fault: The Morphotectonic Expression of a East Slipping Transform Boundary, J. Geophys. Res. 91, 3455-3467, doi:10.1029/JB091iB03p03455.

Gregg, P. M., J. Lin, M. D. Behn, and L. G. J. Montesi (2007), Spreading rate dependence of gravity anomalies along oceanic transform faults. Nature, 448, 183–187, doi:10.1038/nature05962.

Grevemeyer, I. (2020), Upper mantle structure beneath the Mid-Atlantic Ridge from regional waveform modeling, Bull. Seismol. Soc. Am. 110, 18–25, doi:10.1785/0120190080117.

Grevemeyer, I., Reston, T.J., and Moeller, S. (2013), Microseismcity of the Mid-Atlantic Ridge at 7-8.25 S and at the Logatchev Massif oceanic core complex at 14.75N, Geochem. Geophys. Geosyst., v. 14, p. 3532–3554, doi:10.1002/ggge.20197.

Grevemeyer, I., Ranero, C.R., and Ivandic, M. (2018), Structure of oceanic crust and serpentinization at subduction trenches: Geosphere, 14(2), 395–418, doi:10.1130/GES01537.1.

Grevemeyer, I., Hayman, N.W., Lange, D., Peirce, C., Papenberg, C., Van Avendonk, H.J.A., Schmid, F., Gómez de La Peña, L., and Dannowski, A., 2019, Constraining the maximum depth of brittle deformation at slow- and ultraslow-spreading ridges using microseismicity, Geology, 47, 1069–1073, doi:10.1130/G46577.1.

Grevemeyer, I., L. Ruepke, J.P. Morgan, K. Iyer, and C.W. Devey (2021), Extensional tectonics and two-stage crustal accretion at oceanic transform faults, Nature, 591, 402-407, doi:10.1038/s41586-021-03278-9.

Havskov, J., and L. Ottemöller (2000), SEISAN earthquake analysis software, Seismol. Res. Lett., 70, 532–534.

Ligi, M., E. Bonatti, L. Gasperini, and A.N.B. Poliakov (2002), Oceanic broad multifault transform plate boundaries, Geology, 30, 11–14.

Lin, J., and J. P. Morgan (1992), The spreading rate dependence of three-dimensional mid-ocean ridge gravity structure, Geophys. Res. Lett., 19, 13-16, doi:10.1029/91GL03041.

Lonsdale, P. (1986), Tectonic and magmatic ridges in the Eltanin fault system, South Pacific, Mar. Geophys. Res., 8, 203-242, doi:10.1007/BF00305484.

Karson, J.A. and H. J. B. Dick (1983), Tectonics of ridge-transform intersections at the Kane fracture zone, Mar. Geophys. Res., 6, 51-98, https://doi.org/10.1007/BF00300398

McGuire, J., Collins, J., Gouédard, P. et al. (2012), Variations in earthquake rupture properties along the Gofar transform fault, East Pacific Rise. Nature Geosci 5, 336–341, https://doi.org/10.1038/ngeo1454

Menard, H.W., (1955), Deformation of the northeastern Pacific Basin and the west coast of North America, GSA Bulletin; 66 (9): 1149–1198. doi: https://doi.org/10.1130/0016-7606(1955)66[1149:DOTNPB]2.0.CO;2

Menard, H. W. (1967), Extension of Northeastern-Pacific Fracture Zones, Science, 155, 72-74.

Morgan, J. P. and E. M. Parmentier (1984), Lithospheric stress near a ridge-transform intersection, Geophys. Res. Lett., 11: 113-116. doi:10.1029/GL011i002p00113.

Rabain, A., Cannat, M., Escartín, J., Pouliquen, G., Deplus, C., & Rommevaux-Jestin, C., 2001, Focused volcanism and growth of a slow spreading segment (Mid-Atlantic Ridge, 35°N). Earth and Planetary Science Letters, 185(1-2), 211–224. https://doi.org/10.1016/S0012-821X(00)00371-X

Roland, E., D. Lizarralde, J. J. McGuire, and J. A. Collins (2012), Seismic velocity constraints on the material properties that control earthquake behavior at the Quebrada-Discovery-Gofar transform faults, East Pacific Rise, J. Geophys. Res., 117, B11102, doi:10.1029/2012JB009422.

Rowlett, H. (1981), Seismicity at intersection of spreading centers and transform faults, J. Geophys. Res., 86, 3815-3820.

Sandwell, D. T. (1984), Thermomechanical evolution of oceanic fracture zones, J. Geophys. Res., 89, 11401– 11413, doi:10.1029/JB089iB13p11401.

Sandwell, D.T., R. D. Müller, W. H. F. Smith, E. Garcia1, and R. Francis (2014), New global marine gravity model from CryoSat-2 and Jason-1 reveals buried tectonic structure, Science, 346, 65-67, doi:10.1126/science.1258213

Searle, R.C., M.V. Thomas, and E.J.W. Jones (1994), Morphology and tectonics of the Romanche transform and its environs, Mar. Geophys. Res., 16, 427-453, doi:10.1007/BF01270518.

Sykes, L. R. (1967), Mechanism of earthquakes and nature of faulting on the mid-oceanic ridges, J. Geophys. Res., 72, 2131– 2153, doi:10.1029/JZ072i008p02131.

Tucholke, B. E., and J. Lin (1994), A geological model for the structure of ridge segments in slow spreading ocean crust, J. Geophys. Res., 99, 11937– 11958, doi:10.1029/94JB00338.

Wilcock, W. S. D., G. M. Purdy, and S. C. Solomon (1990), Microearthquake evidence for extension across the Kane transform fault, J. Geophys. Res. 95, 15,439-15,462.

Wilson, J.T. (1965), A New Class of Faults and their Bearing on Continental Drift, Nature, 207, 343–347, doi:10.1038/207343a0.

Wolfe, C. J., Bergman, E. A., and Solomon, S. C. (1993), Oceanic transform earthquakes with unusual mechanisms or locations: Relation to fault geometry and state of stress in the adjacent lithosphere, J. Geophys. Res., 98, 16187– 16211, doi:10.1029/93JB00887.

11 Abbreviations

OTF – oceanic transform fault

RTI – ridge-transform intersection

OBS – Ocean-Bottom-Seismometer

OBH – Ocean-Bottom-Hydrophone

12 Appendices

12.1 Selected Pictures of Shipboard Operations

Fig. 12.1 Deployment of a short-period Ocean-Bottom-Seismometer (OBS) (photo: Helene Hilbert)

Fig. 12.2 Broad-band Ocean-Bottom-Seismometer (OBS) on deck of RV METEOR

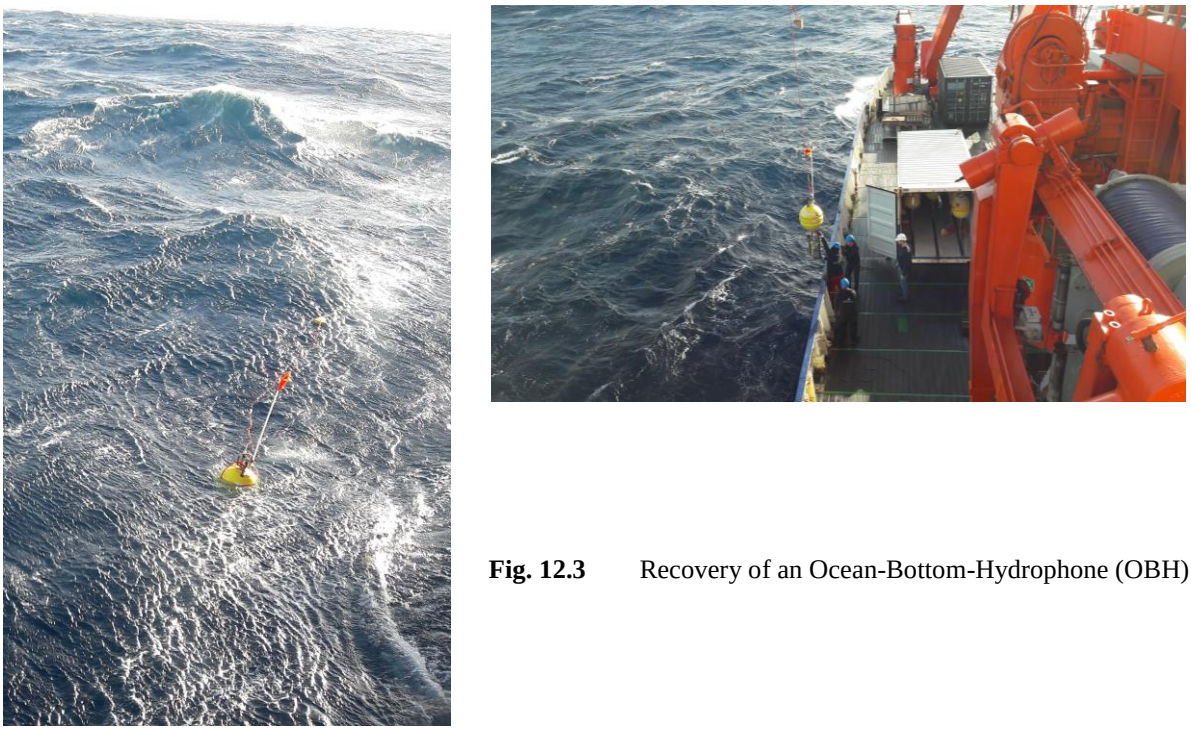

Fig. 12.3 Recovery of an Ocean-Bottom-Hydrophone (OBH)

Fig. 12.4 Dredge with rocks recovered from the Oceanographer transform fault on deck

Fig. 12.5 METEOR rolling in heavy sea (photo: Thies Bartels)